

Article

Numerical Simulation of Nitrogen-Doped Titanium Dioxide as an Inorganic Hole Transport Layer in Mixed Halide Perovskite Structures Using SCAPS 1-D

Nitin Ralph Pochont¹  and Yendaluru Raja Sekhar^{2,*} ¹ School of Mechanical Engineering, Vellore Institute of Technology, Vellore 632014, India² Centre for Disaster Mitigation and Management, Vellore Institute of Technology, Vellore 632014, India

* Correspondence: rajasekhar.y@vit.ac.in

Abstract: Perovskite solar cells (PSCs) stand out as superior third-generation (III-gen) thin-film energy harvesting structures with high efficiency, optical properties and light transmission ability. However, the need to develop cost-effective, stable and sustainable PSCs is allied to the influence of the absorber layer and charge selective transport layers when achieving semi-transparent (ST) structures. Using SCAPS simulation software that can envisage the conceptuality in devising ST PSCs, this work explores and reports the electrical performance of different methylammonium (MA)-based perovskite structures (FTO/TiO₂/PCBM/SnO₂/MAPbI₃/TiO₂:N/PTAA/Spiro-OMeTAD/PEDOT:PSS/Ag). The influence of absorber thickness and defect density is analyzed with optimal parameters. This research reports a novel idea that replaces the polymeric hole transport layer (HTL), such as Spiro-OMeTAD, PEDOT:PSS and PTAA with an air-stable inorganic metal oxide, viz., nitrogen-doped titanium dioxide (TiO₂:N). The simulation results depict an attainable power conversion efficiency of 9.92%, 10.11% and 11.54% for the proposed structures with the novel HTL that are on par with polymeric HTLs. Furthermore, the maximum allowable absorber thickness was 600 nm with a threshold defect density of $1 \times 10^{15} \text{ cm}^{-3}$. The optimized electrical parameters can be implemented to develop thin-film light transmission perovskite cells with rational power conversion efficiencies.

Keywords: nitrogen-doped titanium dioxide; inorganic layer; absorber thickness; defect density; electrical parameters; SCAPS simulation; semi-transparent perovskite cells



Citation: Pochont, N.R.; Sekhar, Y.R. Numerical Simulation of Nitrogen-Doped Titanium Dioxide as an Inorganic Hole Transport Layer in Mixed Halide Perovskite Structures Using SCAPS 1-D. *Inorganics* **2023**, *11*, 3. <https://doi.org/10.3390/inorganics11010003>

Academic Editor: Zemin Zhang

Received: 27 October 2022

Revised: 7 December 2022

Accepted: 8 December 2022

Published: 21 December 2022



Copyright: © 2022 by the authors. Licensee MDPI, Basel, Switzerland. This article is an open access article distributed under the terms and conditions of the Creative Commons Attribution (CC BY) license (<https://creativecommons.org/licenses/by/4.0/>).

1. Introduction

1.1. An Overview of Perovskite Solar Cells

Solar irradiance offers a clean mode of energy production with broad engineering applications. To aspire to the energy sustenance goals for 2030, net-zero emission concepts through renewable sources will foster the achievement of the set targets [1]. In this regard, solar photovoltaics is known to be a prominent renewable source with potential commercial markets. The evolution of solar cells using sophisticated material physics has led to a technological revolution for developing energy generation solutions in diverse applications such as buildings, aircraft and satellites. Photovoltaic solar cells are classified into distinct generations, based on semiconductor raw materials and fabrication techniques, as well as their era of evolution [2]. Substantially, the advent of third-generation solar cells (III-gen SCs) has changed the phase of photovoltaics due to higher power conversion efficiency reaching up to 30%. The significant advantage of III-gen SCs is that one can achieve transparency or semi-transparency, which has paved remarkable novel applications in source integrations [3]. Amongst the different III-gen SCs, perovskite solar cells (PSCs) have gained tremendous interest in the last decade due to their high efficiencies compared to their other counterparts. PSCs' optical and electrical properties include direct and tunable bandgap, high absorption coefficient and longer charge carrier diffusion length [4]. Researchers have developed unique recipes that achieved a power conversion efficiency

(PCE) of 25.2%, which was the apex reported in 2020 [5]. Further findings reveal that PSCs can reach an efficiency of 26.1%, and a multi-junction PSC with a Si-tandem structure attained a PCE of 29.8% [2].

Over the years, the perovskite ABX_3 structure has evolved into a concoction of various elemental combinations [6]. The multi-element ABX_3 system of a PSC comprises diverse metal halide organic and inorganic elements, Figure 1. Methylammonium lead halide ($MAPbX_3$) and formamidinium lead halide ($FAPbX_3$) are the most endorsed organic elements in formulating the cell recipe in planar or mesoporous structures. On the other hand, cationic organic elements (MA and FA) have depicted an intrinsically unstable behavior which led to the presage of inorganic cationic elements such as cesium (Cs), rubidium (Rb), francium (Fr), potassium (K), respectively [7,8]. On the other hand, metals (B) and anions (X) are engineered with different organic and inorganic elements because of enhancing stability, light transmission, and cell efficiency [9,10]. Moreover, within the metal elements, the presence of lead (Pb) increases the toxicity of the cell. Henceforth, literature reports several group IVA and VA elements such as tin (Sn), germanium (Ge), antimony (Sb), bismuth (Bi) and silicon (Si) as an ideal replacement in several chemical PSC recipes [4,11,12]. Lastly, the range of anionic elements revolves majorly around chlorine (Cl^-), bromine (Br^-) and iodine (I^-) [13]. While the top conducting electrodes are generally gold (Au) or silver (Ag), and the bottom substrate is an indium-doped tin oxide (ITO) or a fluorine-doped tin oxide (FTO) glass.

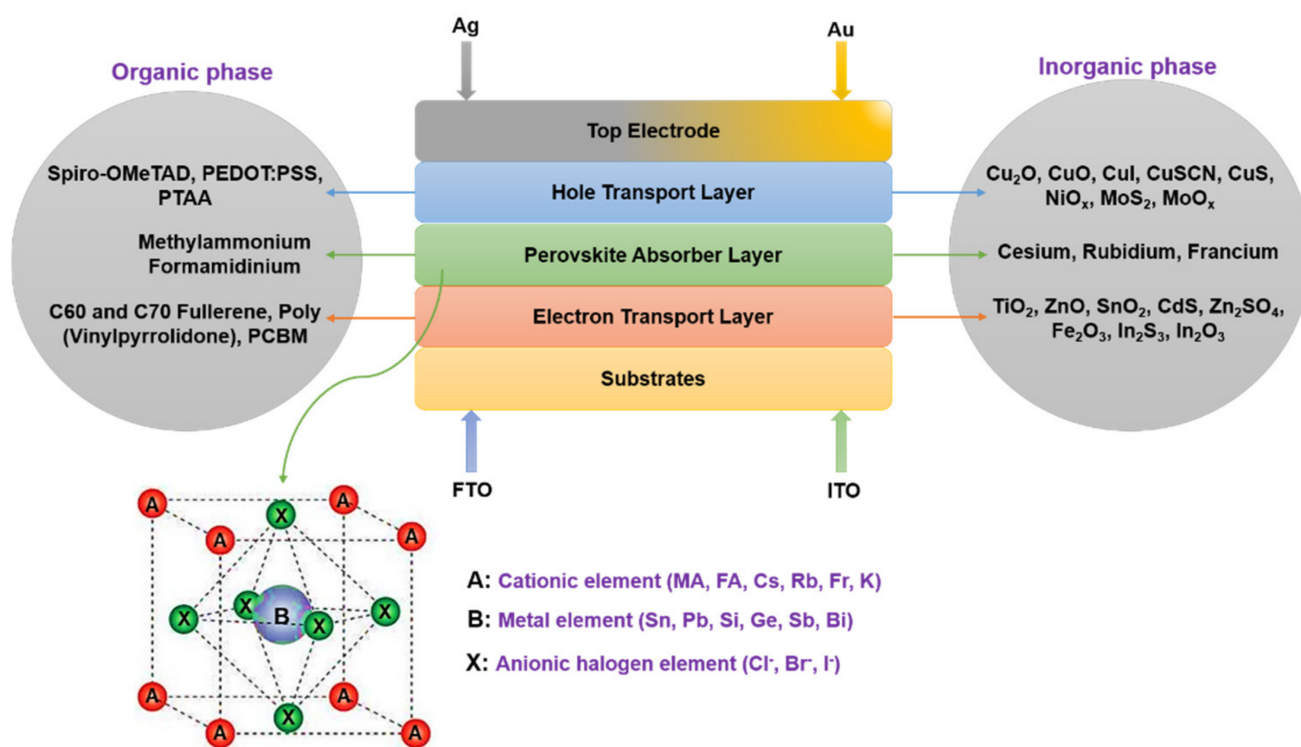


Figure 1. The multi-element structure of a perovskite solar cell.

Charge transport layers in the PSC structure deliver the carrier medium for holes and electrons. The absorber layer is sandwiched between the electron transport layer (ETL) and the hole transport layer (HTL) [14]. The physics behind the transport layers depicts their role in avoiding recombination, preventing cell degradation, boosting charge transportation and efficient light transmission characteristics. The intrinsic absorber layer and the charge transport p-type and n-type layers club to formulate a p-i-n or an n-i-p structure [15]. The transport layers are also deemed to act as blocking layers to their opposite counterparts. The HTLs and ETLs are chosen based on the organic and inorganic material band structure and band edge position. Organic HTLs are advantageous in biodegradability and layer

processing [16], while the drawbacks incurred due to instability, high cost and multi-step synthesis have led to the adoption of inorganic HTLs. In addition, inorganic HTLs promote appealing features such as hole mobility, chemical stability and low-cost [17].

On the other hand, ETLs are chosen based on efficient electron extraction ability and stability. The most common ETLs preferred in a PSC structure are the inorganic-based TiO_2 , ZnO and SnO_2 [18] because of their surface and electrical properties. Furthermore, organic ETLs have less emphasis on the performance output when compared to inorganic ETLs.

1.2. Semi-Transparent Perovskite Solar Cells

Perovskite solar cells acquire exclusive electrical and optical properties such as long charge carrier diffusion length and high absorption coefficient with a direct and tunable bandgap [3]. The organic–inorganic layers in a PSC structure provide an interfacial synergy that nurtures the ability to develop semi-transparent (ST) solar cells. ST PSCs are wavelength perspective structures with the interest of spectral absorbance focused on specific wavelengths in the entire spectrum. In response to the human eye, the average light transparency in the visible range of 400 to 700 nm defines a dimensionless parameter called the average visible transmission (AVT) [19]. The AVT is calculated with the relation [19,20]

$$\text{AVT} = \frac{\int T(\lambda) \cdot P(\lambda) \cdot I(\lambda) \cdot d(\lambda)}{\int T(\lambda) \cdot I(\lambda) \cdot d(\lambda)}$$

where λ —wavelength, T —transmission spectrum, P —photopic response, I —solar flux.

The absorption coefficient in a PSC absorber layer is interlaced with its thickness, which is deemed to reduce to achieve better light transmission properties. However, the reduction in thickness reflects in the drop of open circuit voltage (V_{oc}) and short-circuit current (J_{sc}) [21]. Intuitively, the power conversion efficiency (PCE) holds an inversely proportional behavior to the AVT due to the constraint caused to thinner interfacial layers and wavelength perspective absorbance. Research reports that the PCE is observed to reduce with the increase in the AVT and vice-versa. The key takeaways and strategies that offer the possibilities to attain ST PSCs are illustrated in Figure 2.

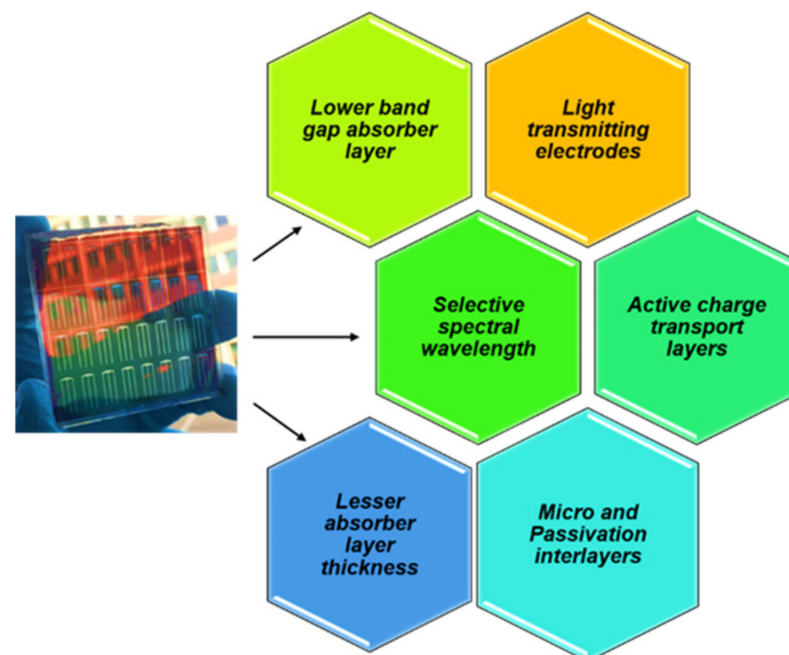


Figure 2. Key takeaways and strategies to attain ST perovskite solar cells [22].

1.3. The Absorber and Charge Transport Layers in an ST PSC

The feasibility of fabricating a stable and efficient ST PSC is possible with molecular engineering of the absorber layer, charge transport layer and conducting electrodes. To achieve efficient electrical and optical properties, researchers worldwide have devised various recipes with a diverse use of elements and their molecular combinations. The absorber layer plays a prime role in delivering efficient outputs. Amongst the different organic/inorganic absorber layers, organic methylammonium lead iodide (MAPbX₃) is considered one of the viable layers that suit the structure of an ST PSC. The modulation of band gap and thickness offers broad characteristics to envisage high electrical properties and light transmission [23]. At even the lowest absorber thickness of 50 nm, MAPbX₃ provides a stable and homogenous layer that can foster high efficiency and high visible light transmission properties [24]. Secondly, the charge transport layers are responsible for the subsistence flow of holes and electrons with no scope for recombination. Due to high light transmission properties, PEDOT: PSS, PTAA and Spiro-OMeTAD are well-known HTLs employed in achieving ST PSCs [25,26]. While visible light-active carbon-loaded anatase titanium dioxide (c-TiO₂) and organic fullerene derivative [6,6]-phenyl-C61-butyric acid methyl ester (PCBM) are well known to have been employed as ETLs to fabricate an ST PSC. The bottom substrates (ITO or FTO) are directly used in the cell structure, but research also reports the possibility of doping the glass substrates with zinc to enhance its strength and bidirectional properties [27–33]. Finally, top electrodes Au or Ag are commonly used, while Au offers better stability from oxidation and a low halide reactivity compared to Ag. Table 1 reports the different ST PSC structures developed in the past decade.

Table 1. ST PSC structures developed in the past decade.

S. No.	Author	ST PSC Device Structure (Top Electrode/HTL/Absorber Layer/ETL/Substrate)	PCE (%)	AVT (%)	Reference	Year
1	Matteocci et al.	ITO/PTAA/MAPbBr _{1-x} Cl _x /c-TiO ₂ /m-TiO ₂ /FTO	64.9	6.3	[28]	2022
2	Ponchai et al.	Au/Spiro-OMeTAD/(PEA) ₂ MA _{n-1} Pb _n Br _{3n+1} /TiO ₂ /FTO	4.86	26.12	[29]	2021
3	Rani et al.	Ag/NiO _x /MAPbI ₃ /TiO ₂ /ZnO/ITO	-	31.49	[30]	2021
4	Singh et al.	Au/PTAA/MAPbBr ₃ /c-TiO ₂ /mp-TiO ₂ /FTO	7.6	52	[31]	2021
5	Zhang et al.	Ag/Zr/PCBM/MAPbI ₃ /NiO _x /ITO	11.74	23	[32]	2021
6	Dew et al.	ITO/Ag/PEDOT: PSS/MAPbI ₃ /PC ₆₁ BM/ITO	7.4	8	[33]	2019
7	Yuan et al.	Ag/ZnO/PC ₆₁ M/MAPbI ₃ /PEDOT: PSS/ITO	8.5	28.4	[22]	2018
8	Han et al.	Ag/PCBM/MAPbI _{3-x} Cl _x /PEDOT: PSS/ITO	13.27	16.3	[34]	2018
9	Chen et al.	Au/Spiro-OMeTAD/MAPbI ₃ /TiO ₂ /FTO	11.7	36	[35]	2016
10	Hö rantner et al.	Au/Spiro-OMeTAD/MAPbI ₃ /c-TiO ₂ /FTO	6.1	38	[36]	2016
11	Lee et al.	Ag/PEDOT: PSS/MAPbI ₃ /PCBM/C ₆₀ /ITO	8.2	34	[37]	2016
12	Chang et al.	Ag/PEDOT: PSS/MAPbI ₃ /PC ₆₁ BM/ITO	11.8	20.8	[38]	2016
13	Heo et al.	Ag/ZnO/PC ₆₁ BM/MAPbI _{3-x} Cl _x /PEDOT: PSS/ITO	7.8	37	[39]	2016
14	Heo et al.	Au/Spiro-OMeTAD/MAPbI ₃ /c-TiO ₂ /mp-TiO ₂ /FTO	4.9	19	[40]	2015
15	Della Gaspera et al.	SnO _x /Ag/PEDOT: PSS/MAPbI ₃ /PCBM/ITO	11.8	29	[24]	2015
16	Eperon et al.	ITO/PEDOT: PSS/PTAA/MAPbI ₃ /TiO ₂ /FTO	10.6	20.9	[41]	2014
17	Lynn et al.	Au/Spiro-OMeTAD/MAPbI ₃ /c-TiO ₂ /FTO	3.5	30	[42]	2012

1.4. Nitrogen-Doped Titanium Dioxide—A Proposed Novel HTL

Titanium dioxide (TiO₂) emerges as a prevalent low-cost photocatalyst with chemical stability and nontoxicity [43]. The cationic or anionic doping modifies this material's bandgap, optical and electrical properties [44]. With tunable bandgap and fermi-level shift, TiO₂ doped with various elements has been demonstrated to be a promising charge transport layer with improved efficiency and open-circuit voltage (V_{oc}) [45]. Literature reports TiO₂ as an ETL in the PSC recipe, but this transport layer perseveres with a limitation of poor visible light absorption. Nitrogen is a suitable doping element in TiO₂ that forms a metastable center, reduced atom size, and low ionization energy [46]. In the recent past, Panepinto et al. [47] reported a breakthrough in devising a nitrogen-doped TiO₂ (TiO₂:N)

layer as an HTL for application in dye-sensitized solar cells. The TiO₂:N HTL layer was fabricated by co-reactive magnetron sputtering and tuning of O₂ and N₂ reactive gas mixture. The doping concentration (%) of nitrogen determines the tunable bandgap of the HTL. Although the usage of TiO₂:N as a low-cost HTL in perovskite solar cell structures has not been explored so far, with enhanced photocatalytic properties, the applicability of TiO₂:N as a stable and low-cost HTL is suitable for semi-transparent PSCs.

1.5. Overview of This Research

This research aims to simulate the charge characteristics and reports the electrical performance of a proposed ST PSC structure with TiO₂:N as the HTL medium. The literature reported in Table 1 quantifies the persistent ETLs (TiO₂, PCBM and SnO₂) and polymeric HTL (Spiro-OMeTAD, PEDOT: PSS and PTAA) mediums used in an ST PSC structure, while oxide-based HTL remains scarce. Since the polymeric HTLs are unstable in nature and high in cost, adopting TiO₂:N as an HTL would deliver an air-stable charge transport medium; this concept has not been performed earlier. Henceforth, the idea of simulating a planar MAPbI₃-based perovskite structure with a comparative analysis (nine different structures) is reported through this research. This study investigates the suitability of the proposed HTL and reports the results obtained by choosing the optimum electrical parameters that can be used when developing an ST PSC practically. These simulation results can be inherited to fabricate a stable and efficient PSC structure with light transmission properties.

2. Results and Discussion

Considering the electrical parameters proposed in the methodology from Section 3.3, with no resistances and dark current, these numerical simulations were performed to estimate the performance output for the proposed PSC. The results attained through SCAPS simulation are presented in Table 2, while the current–voltage characteristics of the PSC structures are displayed in Figure 3a–c.

Table 2. Electrical parametric output attained from the simulation results.

Device Structure	V _{oc} (V)	J _{sc} (mA/cm ²)	FF (%)	PCE (%)
FTO/TiO ₂ /MAPbI ₃ /TiO ₂ :N/Ag	1.07	11.35	81.09	9.92
FTO/TiO ₂ /MAPbI ₃ /Spiro-OMeTAD/Ag	1.10	11.30	80.30	10.00
FTO/TiO ₂ /MAPbI ₃ /PTAA/Ag	1.08	11.32	82.00	10.12
FTO/TiO ₂ /MAPbI ₃ /PEDOT: PSS/Ag	1.08	13.09	83.00	11.75
FTO/PCBM/MAPbI ₃ /TiO ₂ :N/Ag	1.10	12.48	83.32	11.54
FTO/PCBM/MAPbI ₃ /PTAA/Ag	1.12	12.46	83.75	11.73
FTO/PCBM/MAPbI ₃ /Spiro-OMeTAD/Ag	1.13	12.44	83.55	11.77
FTO/PCBM/MAPbI ₃ /PEDOT: PSS/Ag	1.11	13.66	82.71	12.58
FTO/SnO ₂ /MAPbI ₃ /TiO ₂ :N/Ag	1.08	11.33	82.00	10.11
FTO/SnO ₂ /MAPbI ₃ /Spiro-OMeTAD/Ag	1.11	11.28	81.62	10.23
FTO/SnO ₂ /MAPbI ₃ /PEDOT: PSS/Ag	1.10	11.31	86.84	10.89
FTO/SnO ₂ /MAPbI ₃ /PTAA/Ag	1.09	13.08	82.94	11.84

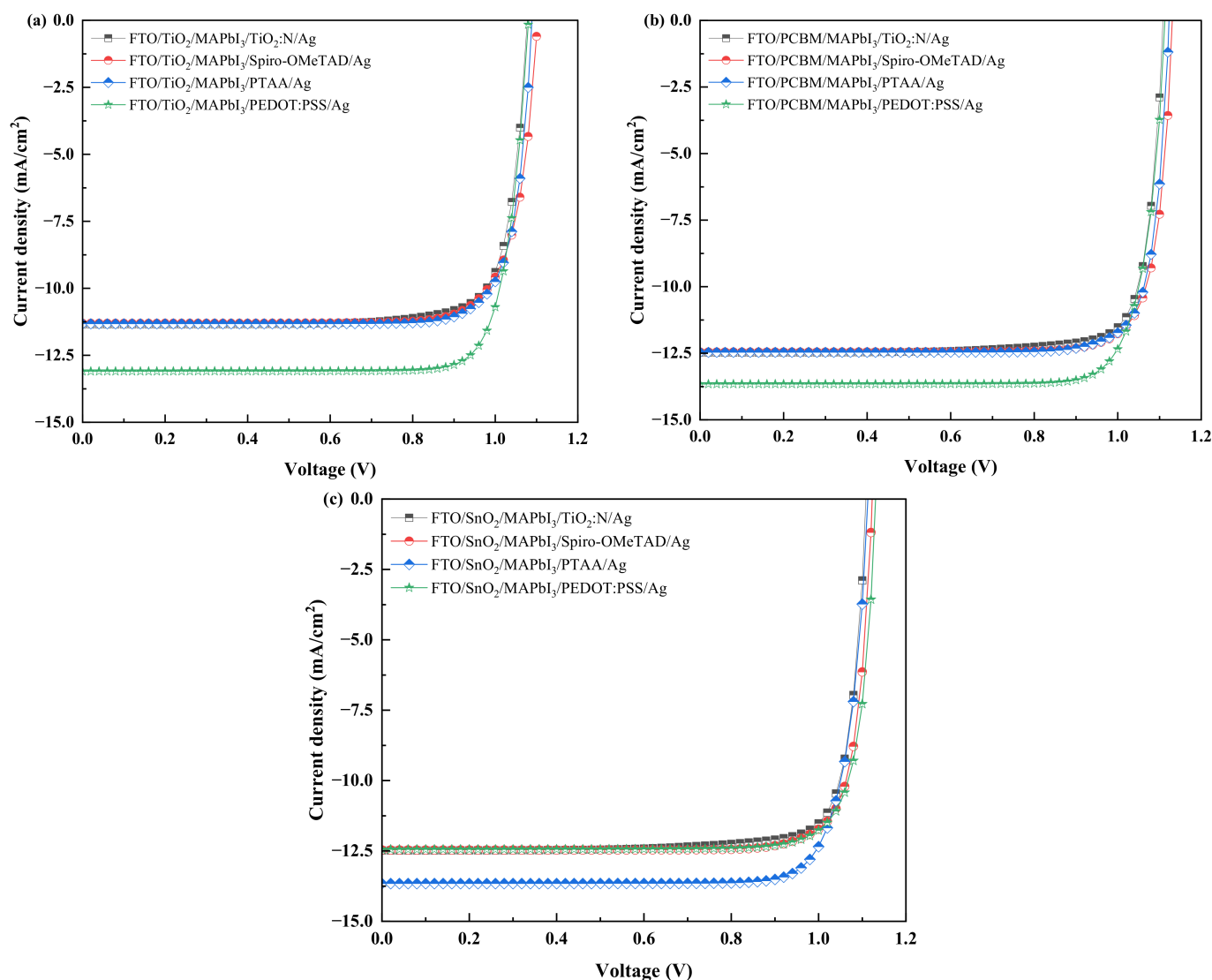


Figure 3. J-V characteristics of the PSC structures with four HTLs and the ETL as: (a) TiO₂ (b) PCBM. (c) SnO₂.

The results infer the significance of N-doped TiO₂ as an HTL with reasonable PCE attained compared to the other HTL structures. However, from Table 2, it is observed for all three cases of ETLs, TiO₂:N as an HTL delivered a lesser PCE (%) when compared to Spiro-OMeTAD, PEDOT: PSS and PTAA. Interestingly though, TiO₂:N as HTL depicted a PCE close to Spiro-OMeTAD and PTAA with a minor difference between 0.08% and 0.23% in the case of TiO₂ and PCBM as the ETL layer, while a comparatively higher drop in PCE of 1.83% and 1.04% was observed when equated to PEDOT: PSS as the HTL layer. In the case of SnO₂ as the ETL layer, simulation results depict a minor drop in PCE of 0.12% and 0.78% when employed with Spiro-OMeTAD and PEDOT: PSS as the HTL layers. However, PTAA as an HTL resulted in a PCE of 1.73% more than TiO₂:N, respectively. These results quantify the role of lesser effective density of states in conduction and valence bands and also the lower shallow acceptor density of TiO₂:N.

2.1. Influence of Absorber Layer Thickness on the Electrical Performance

From the previous section, it is prevalent that a TiO₂:N-based HTL is viable for producing efficiencies on par with polymeric HTLs. In this section, further numerical simulations are carried out to investigate the performance output for the proposed TiO₂:N-based HTL recipes when the absorber layer thickness varies beyond 100 nm. The PCE is

one of the vital factors expected to invariably respond to the degree of change in absorber layer thickness. Hence, this attempt would project the optimum and maximum thickness of the absorber layer to yield better output. The primary electrical parameters from Section 3.3 are considered while the absorber layer thickness is varied proportionally from 100 nm until the saturation level and maximum allowable thickness is observed. Simulations were carried out to analyze the electrical parameters when the HTL layer thickness was varied from 50 nm to 500 nm. The power conversion efficiency (PCE, %) and open circuit voltage (V_{oc} , V) were observed to have no change in their output, while minor differences were observed in the short circuit current (J_{sc} , mA/cm²) and fill factor (FF, %). Hence, the least HTL thickness of 50 nm is considered for this simulation.

Conceptually, the increase in the absorber layer thickness influences the performance parameters of a PSC. With the increase in thickness, J_{sc} tends to increase, since it is attributed to more electron-hole pairs in the absorber layer. In contrast, the V_{oc} decreases due to the increment in the dark saturation current that increases the recombination of charge carriers. Seemingly, the FF holds an inversely proportional relationship with an increase in thickness due to the increase in series resistance and internal power dissipation. Lastly, the PCE increases with thickness but decreases beyond a saturation level (maximum diffusion length). Beyond the saturation point, the fill factor is reported to drop due sheet resistance of the active layer, which is a material perspective phenomenon [48,49].

The simulation results show the performance profile for all the three TiO₂:N-based HTL structures (FTO/TiO₂/MAPbI₃/TiO₂:N/Ag, FTO/PCBM/MAPbI₃/TiO₂:N/Ag and FTO/SnO₂/MAPbI₃/TiO₂:N/Ag) have depicted divergent patterns. Photovoltaic parameters report a change when the absorber layer thickness varies. The attained performance parameters for these recipes are tabulated in Table 3, with the patterns collectively presented in Figure 4. The results depict valid conceptual behavior in the aspect of electrical performance. For these recipes, 600 nm of absorber thickness was observed as the saturation point as indicated in Figure 5, beyond which the PCE and V_{oc} were observed to drop gradually, mainly due to thermal recombination and sheet resistance of the absorber layer. For every interval of increase in absorber layer thickness, the recipe with PCBM as the ETL has been reported to produce higher outputs when compared to TiO₂ and SnO₂-based ETL recipes. In addition, numerical simulations were carried out to analyze these structures' performance when the HTL and ETL thickness was increased. Remarkably, the performance parameters remain unchanged with the increase in HTL thickness, but the increase in ETL thickness was observed to reduce the PCE by a fraction of 0.02% to 0.04%. Hence, the lower thickness of 50 nm was maintained for both the HTL and ETL throughout the simulation process.

Table 3. Performance parameters for both recipes with varied absorber thickness.

PSC Structure	Thickness (nm)	V_{oc} (V)	J_{sc} (mA/cm ²)	FF (%)	PCE (%)
FTO/TiO ₂ /MAPbI ₃ /TiO ₂ :N/Ag	100	1.07	11.35	81.09	9.92
	200	1.05	17.20	78.48	14.30
	300	1.04	20.48	77.26	16.54
	400	1.03	22.40	76.39	17.69
	500	1.02	23.58	75.50	18.24
	600	1.01	24.33	74.57	18.43
	700	1.00	24.82	73.54	18.41

Table 3. Cont.

PSC Structure	Thickness (nm)	V_{oc} (V)	J_{sc} (mA/cm ²)	FF (%)	PCE (%)
FTO/PCBM/MAPbI ₃ /TiO ₂ :N/Ag	100	1.10	12.48	83.32	11.54
	200	1.07	17.66	79.58	15.12
	300	1.05	20.64	77.64	16.93
	400	1.04	22.42	76.59	17.90
	500	1.03	23.53	75.74	18.37
	600	1.02	24.25	74.81	18.53
	700	1.01	24.72	73.83	18.49
FTO/SnO ₂ /MAPbI ₃ /TiO ₂ :N/Ag	100	1.08	11.33	82.00	10.11
	200	1.06	17.19	78.95	14.46
	300	1.04	20.47	77.42	16.64
	400	1.03	22.40	76.49	17.77
	500	1.02	23.58	75.61	18.31
	600	1.01	24.32	74.59	18.53
	700	1.01	24.81	73.68	18.48

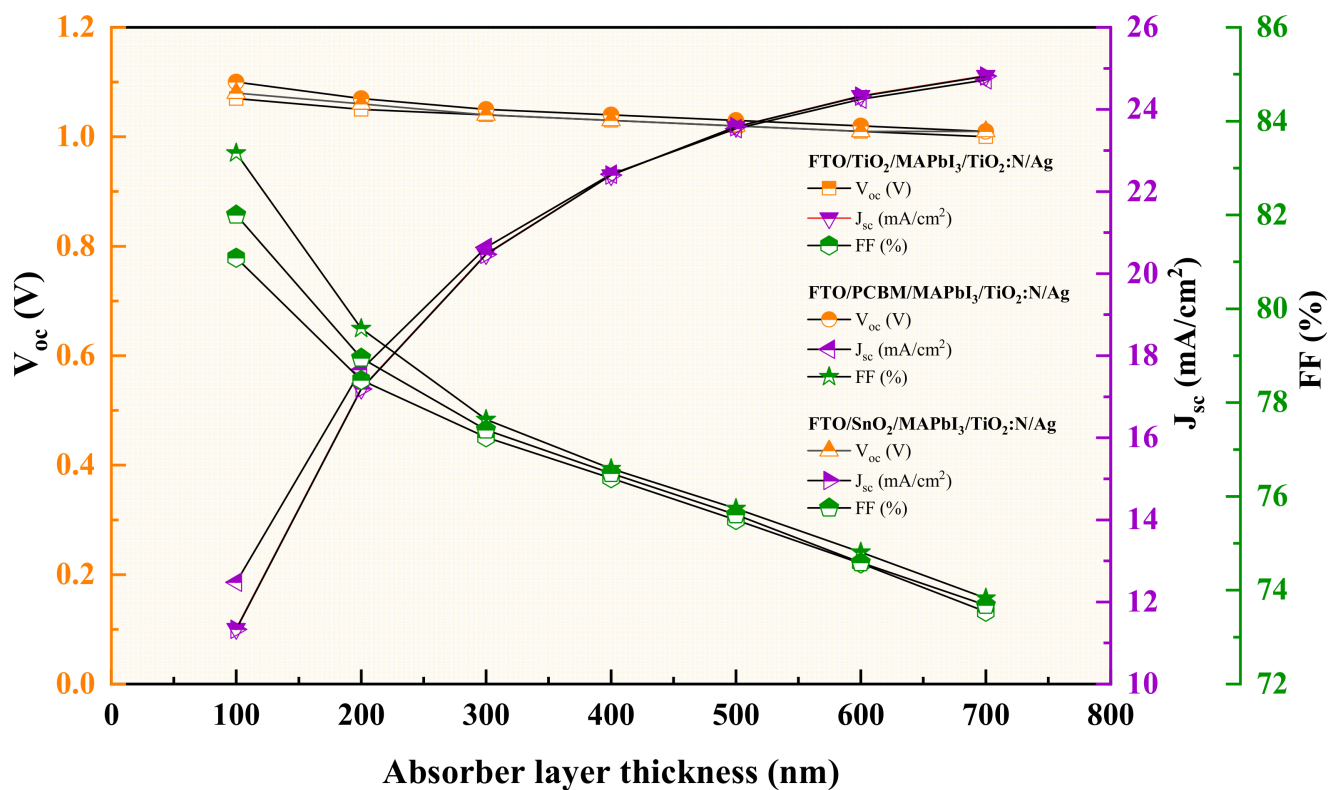


Figure 4. Patterns of the performance parameters for different absorber layer thickness.

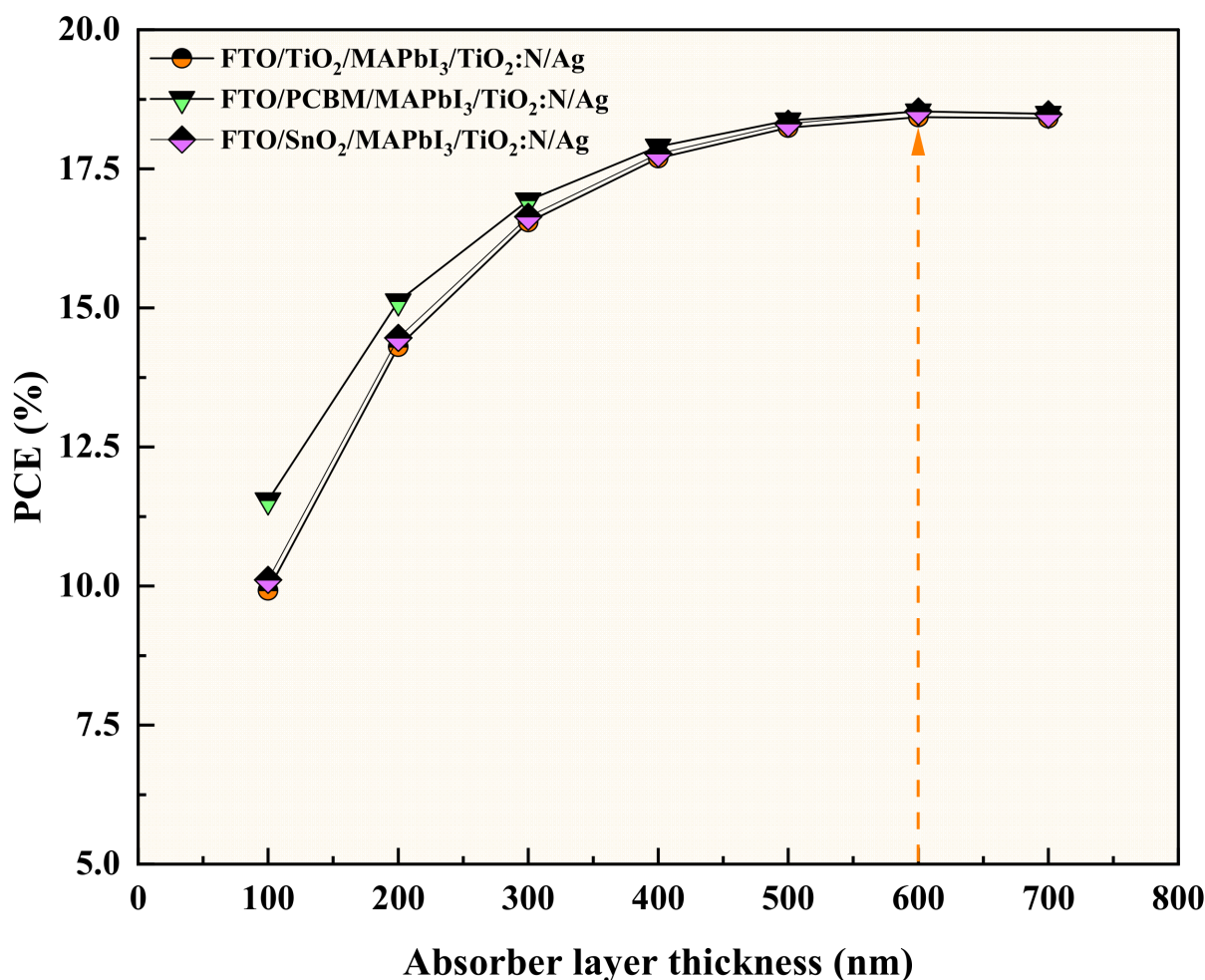


Figure 5. Efficiency curves for a gradient in absorber layer thickness indicating the threshold limit of 600 nm.

2.2. Influence of Absorber Layer Defect Density on the Electrical Performance

The quality and structure of the PSC absorber layer plays a significant role in delivering efficient power outputs. The performance parameters are influenced by the defect density (N_t) of the absorber layer that correlates to the film quality deterioration. This phenomenon causes a density trap and rise in the recombination of charge carriers, which reflects on the cell output [50]. Madan et al. [51] described that the defect densities on the perovskite/ETL and the perovskite/HTL directly influence the performance of the PSC. The effect is more intense when light is illuminated from the ETL side due to the high rate of photons being absorbed near the perovskite/ETL interface. This research investigates and reports the impact of defect density from the perovskite/ETL side as the illumination is projected from the ETL side. Hence, this simulation studies the performance of both the proposed perovskite recipes with a gradient in defect density (N_t) from 1×10^{13} to $1 \times 10^{17} \text{ cm}^{-3}$ for the lower absorber thickness of 100 nm.

The J-V characteristics for the three recipes are reported in Figure 6a–c. Furthermore, the results of this simulation notify a consequent drop in the performance output parameters as the absorber defect density was increased, as reported in Table 4. The simulation results for both recipes infer the impact of the N_t on the PCE (%). With the increase in defect density by $1 \times 10^1 \text{ cm}^{-3}$, the J_{sc} , FF and V_{oc} were observed to reduce logarithmically, resulting in a drop in the PCE (%) in the three recipes. For every degree of rising in the " N_t " by $1 \times 10^1 \text{ cm}^{-3}$, the average efficiency drop was observed to be 1.84% for the FTO/TiO₂/MAPbI₃/TiO₂:N/Ag structure, 2.29% for the FTO/PCBM/MAPbI₃/TiO₂:N/Ag

structure and 1.90% for the FTO/SnO₂/MAPbI₃/TiO₂:N/Ag structure. This pattern infers the disadvantage of using PCBM as the ETL compared to TiO₂:N and SnO₂. However, it is observed that the increase in defect density has a lesser influence on the J_{sc}, but the V_{oc} was observed to respond in proportional change. Interestingly, the J_{sc} remained constant for the N_t of 1 × 10¹⁵ cm⁻³ for both recipes. Beyond 1 × 10¹⁵ cm⁻³ of defect density, these recipes have reported a gradual drop in the electrical parameters reflected in the PCE (%). Henceforth, these simulations conclude the threshold for the absorber layer defect density is 1 × 10¹⁵ cm⁻³ for these respective recipes. The drift in the patterns plotted in Figure 6a–c; notifies that the converging trend is observed for a defect density of 1 × 10¹⁵ cm⁻³ and further.

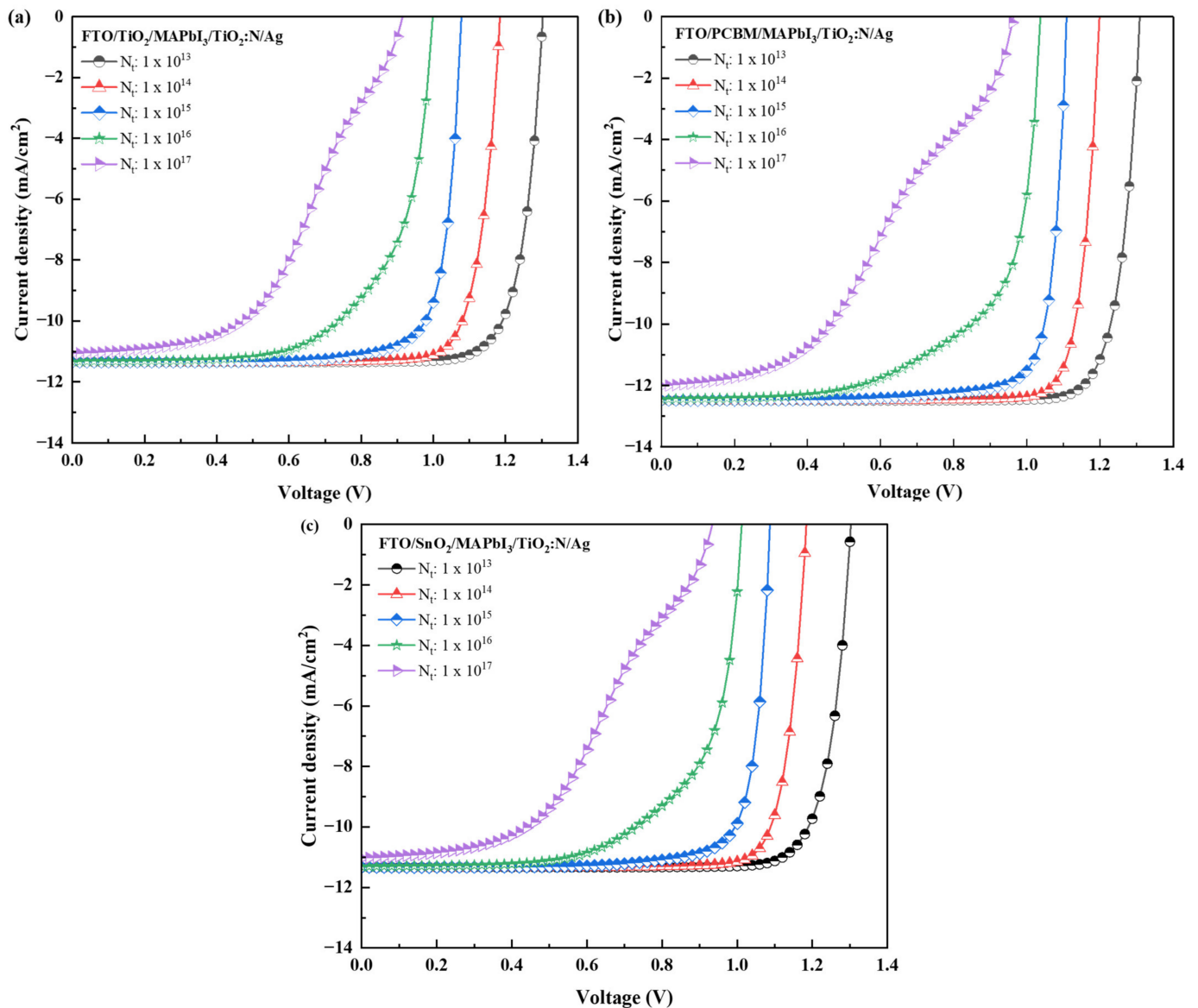


Figure 6. J–V characteristics of the PSC structures with TiO₂:N as HTL and TiO₂ as ETL (a); PCBM as ETL (b); and SnO₂ as ETL (c) layers.

Table 4. Performance parameters for proposed recipes with a gradient in defect density.

Recipe	Absorber Layer Defect Density (N_t , cm^{-3})	V_{oc} (V)	J_{sc} (mA/cm^{-2})	FF (%)	PCE (%)
FTO/TiO ₂ /MAPbI ₃ /TiO ₂ :N/Ag	1×10^{13}	1.30	11.35	83.42	12.34
	1×10^{14}	1.18	11.35	83.74	11.26
	1×10^{15}	1.07	11.35	81.09	9.92
	1×10^{16}	0.99	11.32	65.63	7.42
	1×10^{17}	0.91	11.07	49.18	4.98
FTO/PCBM/MAPbI ₃ /TiO ₂ :N/Ag	1×10^{13}	1.30	12.48	84.79	13.86
	1×10^{14}	1.19	12.48	85.87	12.85
	1×10^{15}	1.10	12.48	83.32	11.54
	1×10^{16}	1.03	12.43	66.05	8.52
	1×10^{17}	0.96	12.02	40.62	4.70
FTO/SnO ₂ /MAPbI ₃ /TiO ₂ :N/Ag	1×10^{13}	1.30	11.33	83.69	12.36
	1×10^{14}	1.18	11.33	84.80	11.39
	1×10^{15}	1.08	11.33	82.00	10.11
	1×10^{16}	1.02	11.30	65.08	7.45
	1×10^{17}	0.93	11.03	45.99	4.74

Additionally, further numerical simulations were carried out to study the influence caused on the efficiency of the defect density of HTL and ETL layers. The N_t was varied from 1×10^3 to $1 \times 10^7 \text{ cm}^{-3}$ for the transport layers. The simulation results have reported no change in the performance of either PSC structure. This denotes the influence of defect density susceptible to the perovskite absorber layer only.

3. Methodology

3.1. SCAPS Software Simulation

The solar cells capacitance simulator (SCAPS 3.10) one-dimensional software is a modern computational tool developed to simulate solar cell physics numerically. SCAPS provides a theoretical understanding of solar cell behavior that helps compare results with experimental analysis [52]. The SCAPS built-in program is designed to numerically solve semiconductor equations in 1D steady-state conditions. Global researchers recognized SCAPS as a suitable analytical tool to determine I-V characteristics, fill factor, band diagrams, quantum efficiencies, spectral responses, short-circuit current and open-circuit voltage, PCE and recombination profile within the charge transport layers [53–55]. The performance of the fabricated solar cell is based on the semiconductor Equations (1)–(6);

$$\text{Electron continuity eqn., } \frac{dn_p}{dt} = G_n - \frac{n_p - n_{p0}}{\tau_n} + n_p \mu_n \frac{d\xi}{dx} + \mu_n \xi \frac{dn_p}{dx} + D_n \frac{d^2 n_p}{dx^2} \quad (1)$$

$$\text{Hole continuity eqn., } \frac{dp_n}{dt} = G_p - \frac{p_n - p_{n0}}{\tau_p} - p_n \mu_p \frac{d\xi}{dx} - \mu_p \xi \frac{dp_n}{dx} + D_p \frac{d^2 p_n}{dx^2} \quad (2)$$

$$\text{Poissons eqn., } \frac{d}{dx} \left(-\varepsilon(x) \frac{d\psi}{dx} \right) = q [p(x) - n(x) + N_d^+(x) - N_a^-(x) + p_t(x) - n_t(x)] \quad (3)$$

On a more fundamental basis, an alternative way to express the equations was presented by [56]. Equation (3) is also described as;

$$\frac{d^2}{dx^2} \psi(x) = \frac{q}{\varepsilon} [p(x) - n(x) + N_D - N_A + p_h - p_e] \quad (4)$$

$$\frac{dJ_n}{dx} = G - R \quad (5)$$

$$\frac{dJ_p}{dx} = G - R \quad (6)$$

3.2. $\text{TiO}_2\text{:N}$ as a p-Type HTL

As an alternative to expensive HTLs, this research examines the applicability and feasibility of implementing $\text{TiO}_2\text{:N}$ as an HTL in a PSC recipe. Several studies revealed that N-doped TiO_2 exhibits stable p-type conductivity. Towards analyzing the cation vacancies in TiO_2 , Lee et al. [57] reported that n-type TiO_2 and p-type TiO_2 exhibit similar morphology, surface area and crystal structure. Comparatively, p-type TiO_2 has better stability and performance rate. Vasu et al. [58] employed the atomic layer deposition technique to develop a p-type epitaxial N-doped TiO_2 thin film. The results depict a reduced optical bandgap and better hole concentration and mobility. Vasilopoulou et al. [59] stated that p-type nitrogen doping enhances the photocatalytic efficiency of TiO_2 in the visible spectrum, while Anitha et al. [60] reported that the charge transportation could be eased in TiO_2 due to additional bands, which can be achieved through cationic doping. Researchers synthesized the p-type $\text{TiO}_2\text{:N}$ film with different nitrogen doping concentrations. As the N-doping increases, results depicted a change in light transmittance (%), optical bandgap (E_g), Hall coefficient (cm^3/C), carrier density (cm^{-3}), conductivity ($\Omega^{-1}\cdot\text{cm}^{-1}$) and mobility ($\text{cm}^2\cdot\text{v}^{-1}\cdot\text{s}^{-1}$). In addition, a further increase in nitrogen concentration would lead to a short-circuit in the cell, making it inappropriate as a photocathode. Literature studies inferred that TiO_2 has a tunable bandgap nature that depends on the nitrogen concentration [59,60].

3.3. The Proposed Perovskite Solar Cell Structure

This research simulates a PSC recipe developed with methylammonium lead iodide (MAPbI_3) as the absorber layer. Various charge transport layers are considered to investigate the performance, and the optimum high responsive match in electrical performance is reported. Certain characteristics of the MA-based absorber layer include the ability of lower thickness, lower bandgap of 1.5 eV, lower defect states, better thermal stability and good optical properties compared to other absorber layers. Hence, MA-based PSCs are considered one of the most promising light-absorbing perovskite materials. Likewise, to validate the electrical behavior of $\text{TiO}_2\text{:N}$ as an HTL, a comparative analysis is carried out in this simulation by adopting two different polymeric HTLs (Spiro-OMeTAD, PEDOT:PSS and PTAA) and ETLs (TiO_2 , PCBM and SnO_2) which tend to possess efficient light transmission properties. These charge transport layers' electrical parameters are optimized according to the parameters adopted from earlier various experimental and simulation studies that reported their significance. SCAPS software simulation for the proposed structures is performed using distant parameters, reported in Table 5. In view of attaining thin-film light transmission solar cells, the thickness of the charge transport layers is considered 50 nm, as the lowest value, which is an attainable thickness from various coating techniques [61]. The planned n-i-p PSC configuration structure is illustrated in Figure 7a. In contrast, the SCAPS simulation design of the proposed structure is pictured in Figure 8. Adopting TiO_2 as HTL is a unique technique for developing a low-cost PSC with higher optical properties. Literature reports that the bandgap and light transmission (%) is significantly reduced as the doping concentration increases.

Table 5. The proposed electrical parameter considered for software simulation of PSC structures [62–71].

Parameters	Substrate		ETL		Perovskite Absorber Layer	Novel HTL	Polymeric HTLs		
	FTO	TiO ₂	PCBM	SnO ₂	MAPbI ₃	TiO ₂ :N	Spiro-OMeTAD	PEDOT: PSS	PTAA
Thickness 't' (nm)	200	50	50	50	100 *	50	50	50	50
Bandgap 'E _g ' (eV)	3.5	3.2	2	3.4	1.55	3	2.88	1.8	2.96
Electron affinity 'χ' (eV)	4	4	3.9	4	3.9	2.2	2.05	3.4	2.3
Dielectric Permittivity 'ε _r '	9	9	4	9	6.5	3	3	3	9
CB EDOS 'N _c ' (cm ⁻³)	2.2 × 10 ¹⁸	2.2 × 10 ¹⁸	1 × 10 ²¹	2.2 × 10 ¹⁸	2.2 × 10 ¹⁹	1.3 × 10 ¹⁴	2.2 × 10 ¹⁸	2.2 × 10 ¹⁸	1 × 10 ²¹
VB EDOS 'N _v ' (cm ⁻³)	2.2 × 10 ¹⁸	1.8 × 10 ¹⁹	2 × 10 ²⁰	1.8 × 10 ¹⁹	1.3 × 10 ¹⁹	1.3 × 10 ¹⁵	1.8 × 10 ¹⁹	1.8 × 10 ¹⁹	1 × 10 ²¹
e ⁻ thermal velocity (cm.s ⁻¹)	1 × 10 ⁷	1 × 10 ⁷	1 × 10 ⁷	1 × 10 ⁷	1 × 10 ⁷	1 × 10 ⁷	1 × 10 ⁷	1 × 10 ⁷	1 × 10 ⁷
h ⁺ thermal velocity (cm.s ⁻¹)	1 × 10 ⁷	1 × 10 ⁷	1 × 10 ⁷	1 × 10 ⁷	1 × 10 ⁷	1 × 10 ⁷	1 × 10 ⁷	1 × 10 ⁷	1 × 10 ⁷
Electron mobility 'μ _n ' (cm ² /V.s)	20	20	1 × 10 ⁻²	20	2.7	2	2 × 10 ⁻⁴	100	1
Hole mobility 'μ _p ' (cm ² /V.s)	10	10	1 × 10 ⁻²	10	1.8	2	2 × 10 ⁻⁴	4	40
Shallow donor density 'N _D ' (cm ⁻³)	2 × 10 ¹⁹	1 × 10 ¹⁶	1 × 10 ²⁰	1 × 10 ¹⁷	1.3 × 10 ¹⁶	0	0	0	0
Shallow Acceptor density 'N _A ' (cm ⁻³)	0	0	0	0	1.3 × 10 ¹⁶	1.3 × 10 ¹⁴	2 × 10 ¹⁹	2 × 10 ¹⁹	2 × 10 ¹⁹
Defect density 'N _t ' (cm ⁻³)	1 × 10 ¹⁵	1 × 10 ¹⁵	1 × 10 ¹⁴	1 × 10 ¹⁵	1 × 10 ¹⁵ *	1 × 10 ¹⁵	1 × 10 ¹⁵	1 × 10 ¹⁴	1 × 10 ¹⁵

* Varied parameter.

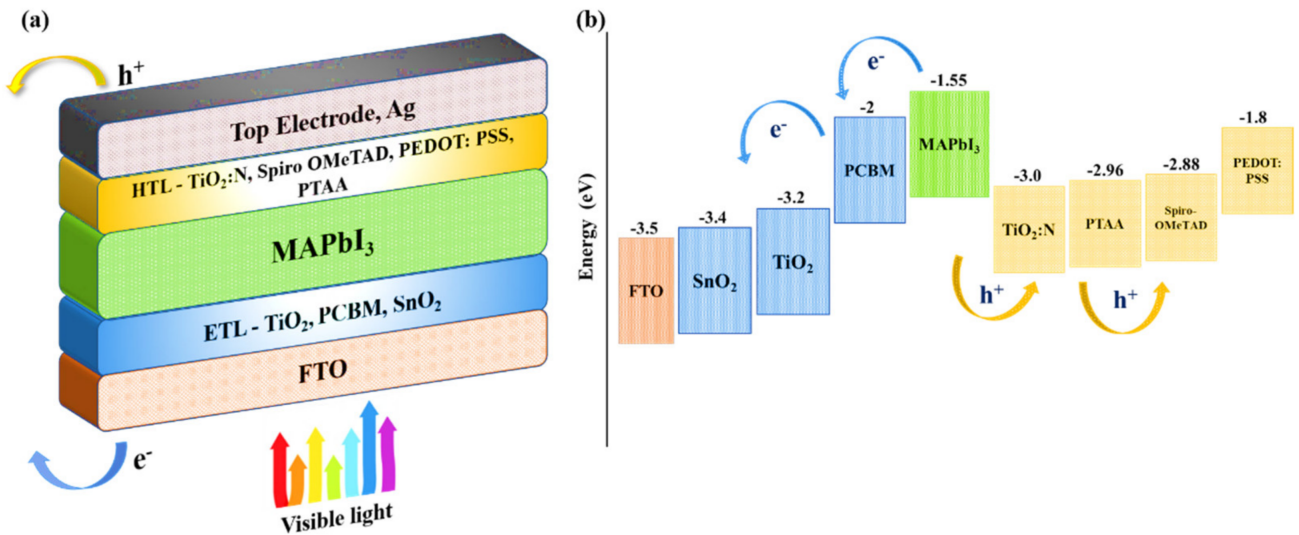


Figure 7. (a) Proposed n–i–p structure of the PSC with different layers. (b) Energy band diagram of the PSC structure (combined) with bandgap denotation for absorber and charge transport layers [62–71].

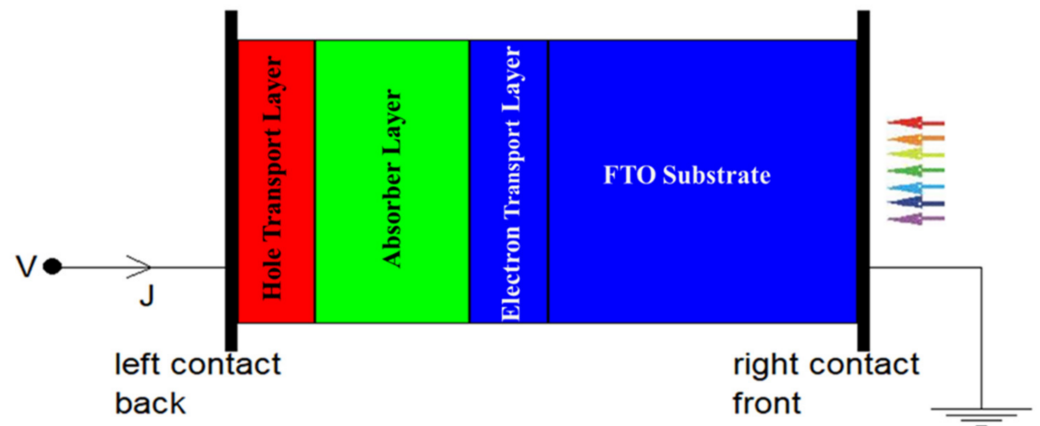


Figure 8. SCAPS simulation design of the PSC structure.

The bandgap of TiO₂:N was optimized by Vasu et al. [58] to develop a p-type epitaxial N-doped TiO₂ thin film. The initial bandgap of bulk anatase n-type TiO₂ was observed to be 3.23 eV; upon doping with 4.0% concentration (from XPS analysis) of nitrogen, the bandgap was deemed to reduce to 3.07 eV in the TiO₂:N film which also reported p-type behavior due to the decrease in the fermi-energy levels. Additionally, from preliminary simulations performed in this research, it was observed that an increase in nitrogen concentration would induce a short-circuit in the cell when the HTL bandgap is less than 2.5 eV. Hence, nitrogen doping levels must be controlled to attain a bandgap of more than 2.5 eV for an ideal HTL medium with optimum light transmission properties. Therefore, considering previous experimental studies, this study investigates the behavior of the PSC structure with a proposed HTL bandgap of 3.0 eV. The energy band diagram for the proposed corresponding layers in the PSC structure is illustrated in Figure 7b. The energy levels in Figure 7b were optimized and reported according to previous experimental data.

4. Conclusions

Among the strategies identified from the reported literature, this study deals with simulating a PSC structure with an absorber layer having a lower bandgap and layer thickness as well as a novel inorganic charge transport medium in the form of N-doped TiO₂. This work proposes the optimal electrical parameters for different MA-based perovskite recipes that can attain rational outputs. SCAPS-1D software simulation has been performed in this study with three specific PSC structures: FTO/TiO₂/MAPbI₃/TiO₂:N/Ag, FTO/SnO₂/MAPbI₃/TiO₂:N/Ag and FTO/PCBM/MAPbI₃/TiO₂:N/Ag, respectively. The present results were validated by simulating the PSC structure with different polymeric HTL and ETL layers available in the literature. The simulation results reveal that the proposed PSC structures with TiO₂:N as an HTL have estimated a PCE of 9.92%, 10.11% and 11.54%, which are on par with other PSC structures employing polymeric HTLs. Simulations reveal that TiO₂:N as an HTL can deliver a PCE on par with Spiro-OMeTAD and PTAA when TiO₂ and PCBM are used as the ETL layers, while it closely matches the PCE of PEDOT: PSS when SnO₂ is employed as the ETL medium. Furthermore, the absorber layer thickness for the proposed recipes was varied from 100 nm to 700 nm in steps of 100 nm, and it was observed that 600 nm was the threshold layer thickness that avoids recombination losses. In addition, the influence of absorber layer defect density on the performance of PSC was analyzed to identify the saturation limit through the drift pattern. Defect density beyond $1 \times 10^{15} \text{ cm}^{-3}$ observed a drop in J_{sc} and, thereby, a reduction in the fill factor. Lastly, the electrical parameters of the proposed mixed metal halide PSC structures with TiO₂:N as an HTL could be used to envisage a semi-transparent perovskite solar cell with the lowest layer thickness, reasonable efficiencies and comparatively lower costs.

Author Contributions: Conceptualization, N.R.P. and Y.R.S.; methodology, N.R.P. and Y.R.S.; validation, N.R.P. and Y.R.S.; investigation, Y.R.S.; writing—original draft preparation, N.R.P.; review and editing, N.R.P. and Y.R.S.; supervision, Y.R.S. All authors have read and agreed to the published version of the manuscript.

Funding: The funding was supported by Vellore Institute of Technology University.

Data Availability Statement: Not applicable.

Acknowledgments: The authors thank Marc Burgelman, ELSI, University of Gent, Belgium, for providing the SCAPS 3.10 version simulation software used in this numerical study. The authors thank Vellore Institute of Technology for supporting the open-access publication fee.

Conflicts of Interest: The authors declare no conflict of interest.

Sample Availability: Samples of the compounds are available from the authors.

Nomenclature

Ψ :	electrostatic potential	p_h :	hole distribution
q :	electric charge	p_e :	electron distribution
ϵ :	dielectric constant	J_n :	current density for electron
p :	hole concentration	J_p :	current density for the hole
n :	electron concentration	G :	Generation rates for carriers
N_D :	doping concentration for the donor	R :	recombination rates for carriers
N_A :	doping concentration for acceptor		

References

- Rao, V.T.; Sekhar, Y.R. Exergo-Economic and CO₂ Emission Analysis of Bi-Symmetrical Web Flow Photovoltaic-Thermal System Under Diurnal Conditions. *J. Energy Resour. Technol.* **2022**, *145*, 032001. [CrossRef]
- Best Research-Cell Efficiency Chart—2022. National Renewable Energy Laboratory (NREL). Available online: <https://www.nrel.gov/pv/cell-efficiency.html> (accessed on 17 October 2022).
- Rahmany, S.; Etgar, L. Semitransparent Perovskite Solar Cells. *ACS Energy Lett.* **2020**, *5*, 1519–1531. [CrossRef]
- Nalinya, M.A.; Awino, C.; Barasa, H.; Odari, V.; Gaitho, F.; Omogo, B.; Mageto, M. Numerical study of lead free CsSn_{0.5}Ge_{0.5}I₃ perovskite solar cell by SCAPS-1D. *Optik* **2021**, *248*, 168060. [CrossRef]
- Liu, G.; Liu, Z.; Wang, L.; Zhang, K.; Xie, X. A combined chrome oxide and titanium oxide-based electron-transport layer for high-performance perovskite solar cells. *Chem. Phys. Lett.* **2021**, *771*, 138496. [CrossRef]
- Park, N.-G. Perovskite solar cells: An emerging photovoltaic technology. *Mater. Today* **2015**, *18*, 65–72. [CrossRef]
- Tai, Q.; Tang, K.-C.; Yan, F. Recent progress of inorganic perovskite solar cells. *Energy Environ. Sci.* **2019**, *12*, 2375–2405. [CrossRef]
- Nam, J.K.; Chai, S.U.; Cha, W.; Choi, Y.J.; Kim, W.; Jung, M.S.; Kwon, J.; Kim, D.; Park, J.H. Potassium Incorporation for Enhanced Performance and Stability of Fully Inorganic Cesium Lead Halide Perovskite Solar Cells. *Nano Lett.* **2017**, *17*, 2028–2033. [CrossRef]
- Chen, C.; Zheng, S.; Song, H. Photon management to reduce energy loss in perovskite solar cells. *Chem. Soc. Rev.* **2021**, *50*, 7250–7329. [CrossRef]
- Zhang, Y.; Grancini, G.; Feng, Y.; Asiri, A.M.; Nazeeruddin, M.K. Optimization of Stable Quasi-Cubic FA_xMA_{1-x}PbI₃ Perovskite Structure for Solar Cells with Efficiency beyond 20%. *ACS Energy Lett.* **2017**, *2*, 802–806. [CrossRef]
- Chiara, R.; Morana, M.; Malavasi, L. Germanium-Based Halide Perovskites: Materials, Properties, and Applications. *ChemPlusChem* **2021**, *86*, 879–888. [CrossRef]
- Correa-Baena, J.-P.; Nienhaus, L.; Kurchin, R.C.; Shin, S.S.; Wiegold, S.; Hartono, N.T.P.; Layurova, M.; Klein, N.D.; Poindexter, J.R.; Polizzotti, A.; et al. A-Site Cation in Inorganic A₃Sb₂I₉ Perovskite Influences Structural Dimensionality, Exciton Binding Energy, and Solar Cell Performance. *Chem. Mater.* **2018**, *30*, 3734–3742. [CrossRef]
- Gkini, K.E.; Antoniadou, M.; Balis, N.; Kaltzoglou, A.; Kontos, A.G.; Falaras, P. Mixing cations and halide anions in perovskite solar cells. *Mater. Today Proc.* **2019**, *19*, 73–78. [CrossRef]
- Shao, S.; Loi, M.A. The Role of the Interfaces in Perovskite Solar Cells. *Adv. Mater. Interfaces* **2019**, *7*, 1901469. [CrossRef]
- Zhou, D.; Zhou, T.; Tian, Y.; Zhu, X.; Tu, Y. Perovskite-Based Solar Cells: Materials, Methods, and Future Perspectives. *J. Nanomater.* **2018**, *2018*, 8148072. [CrossRef]
- Nhari, L.M.; El-Shishtawy, R.M.; Asiri, A.M. Recent progress in organic hole transport materials for energy applications. *Dye. Pigment.* **2021**, *193*, 109465. [CrossRef]
- Wang, Q.; Lin, Z.; Su, J.; Hu, Z.; Chang, J.; Hao, Y. Recent progress of inorganic hole transport materials for efficient and stable perovskite solar cells. *Nano Sel.* **2021**, *2*, 1055–1080. [CrossRef]
- Kim, J.; Kim, K.S.; Myung, C.W. Efficient electron extraction of SnO₂ electron transport layer for lead halide perovskite solar cell. *npj Comput. Mater.* **2020**, *6*, 100. [CrossRef]
- Mujahid, M.; Chen, C.; Zhang, J.; Li, C.; Duan, Y. Recent advances in semitransparent perovskite solar cells. *InfoMat* **2021**, *3*, 101–124. [CrossRef]
- Pulli, E.; Rozzi, E.; Bella, F. Transparent photovoltaic technologies: Current trends towards upscaling. *Energy Convers. Manag.* **2020**, *219*, 112982. [CrossRef]
- You, P.; Liu, Z.; Tai, Q.; Liu, S.; Yan, F. Efficient Semitransparent Perovskite Solar Cells with Graphene Electrodes. *Adv. Mater.* **2015**, *27*, 3632–3638. [CrossRef]
- Yuan, L.; Wang, Z.; Duan, R.; Huang, P.; Zhang, K.; Chen, Q.; Allam, N.K.; Zhou, Y.; Song, B.; Li, Y. Semi-transparent perovskite solar cells: Unveiling the trade-off between transparency and efficiency. *J. Mater. Chem. A* **2018**, *6*, 19696–19702. [CrossRef]
- Wang, G.; Chang, J.; Tang, W.; Xie, W.; Ang, Y.S. 2D materials and heterostructures for photocatalytic water-splitting: A theoretical perspective. *J. Phys. D Appl. Phys.* **2022**, *55*, 293002. [CrossRef]
- Della Gaspera, E.; Peng, Y.; Hou, Q.; Spiccia, L.; Bach, U.; Jasieniak, J.J.; Cheng, Y.-B. Ultra-thin high efficiency semitransparent perovskite solar cells. *Nano Energy* **2015**, *13*, 249–257. [CrossRef]

25. Guchhait, A.; Dalapati, G.K.; Sonar, P.; Gopalan, S.; Bin Suhaimi, F.; Das, T.; Dutt, V.G.V.; Mishra, N.; Mahata, C.; Kumar, A.; et al. p-i-n Structured Semitransparent Perovskite Solar Cells with Solution-Processed Electron Transport Layer. *J. Electron. Mater.* **2021**, *50*, 5732–5739. [[CrossRef](#)]
26. Aharon, S.; Layani, M.; Cohen, B.-E.; Shukrun, E.; Magdassi, S.; Etgar, L. Self-Assembly of Perovskite for Fabrication of Semitransparent Perovskite Solar Cells. *Adv. Mater. Interfaces* **2015**, *2*, 1500118. [[CrossRef](#)]
27. Lim, S.-H.; Seok, H.-J.; Kwak, M.-J.; Choi, D.-H.; Kim, S.-K.; Kim, D.-H.; Kim, H.-K. Semi-transparent perovskite solar cells with bidirectional transparent electrodes. *Nano Energy* **2021**, *82*, 105703. [[CrossRef](#)]
28. Matteocci, F.; Rossi, D.; Castriotta, L.A.; Ory, D.; Mejaouri, S.; der Maur, M.A.; Sauvage, F.; Cacovich, S.; Di Carlo, A. Wide bandgap halide perovskite absorbers for semi-transparent photovoltaics: From theoretical design to modules. *Nano Energy* **2022**, *101*, 107560. [[CrossRef](#)]
29. Ponchai, J.; Srathongsian, L.; Amratisha, K.; Boonthum, C.; Sahasithiwat, S.; Ruankham, P.; Kanjanaboos, P. Modified colored semi-transparent perovskite solar cells with enhanced stability. *J. Alloys Compd.* **2021**, *875*, 159781. [[CrossRef](#)]
30. Rani, S.; Kumar, A.; Ghosh, D.S. High performance of NiO-Ag-NiO based semi-transparent perovskite solar cell. *Mater. Today Proc.* **2022**, *66*, 3224–3227. [[CrossRef](#)]
31. Singh, A.; Matteocci, F.; Zhu, H.; Rossi, D.; Mejaouri, S.; Cacovich, S.; Der Maur, M.A.; Sauvage, F.; Gagliardi, A.; Grätzel, M.; et al. Methylamine Gas Treatment Affords Improving Semitransparency, Efficiency, and Stability of CH₃NH₃PbBr₃-Based Perovskite Solar Cells. *Sol. RRL* **2021**, *5*, 2100277. [[CrossRef](#)]
32. Zhang, Y.-W.; Cheng, P.-P.; Tan, W.-Y.; Min, Y. Balance the thickness, transparency and stability of semi-transparent perovskite solar cells by solvent engineering and using a bifunctional additive. *Appl. Surf. Sci.* **2021**, *537*, 147908. [[CrossRef](#)]
33. Dewi, H.A.; Wang, H.; Li, J.; Thway, M.; Sridharan, R.; Stangl, R.; Lin, F.; Aberle, A.G.; Mathews, N.; Bruno, A.; et al. Highly Efficient Semitransparent Perovskite Solar Cells for Four Terminal Perovskite-Silicon Tandems. *ACS Appl. Mater. Interfaces* **2019**, *11*, 34178–34187. [[CrossRef](#)]
34. Han, K.; Xie, M.; Zhang, L.; Yan, L.; Wei, J.; Ji, G.; Luo, Q.; Lin, J.; Hao, Y.; Ma, C.-Q. Fully solution processed semi-transparent perovskite solar cells with spray-coated silver nanowires/ZnO composite top electrode. *Sol. Energy Mater. Sol. Cells* **2018**, *185*, 399–405. [[CrossRef](#)]
35. Chen, B.-X.; Rao, H.-S.; Chen, H.-Y.; Li, W.-G.; Kuang, D.-B.; Su, C.-Y. Ordered macroporous CH₃NH₃PbI₃ perovskite semitransparent film for high-performance solar cells. *J. Mater. Chem. A* **2016**, *4*, 15662–15669. [[CrossRef](#)]
36. Hörantner, M.T.; Nayak, P.K.; Mukhopadhyay, S.; Wojciechowski, K.; Beck, C.; McMeekin, D.; Kamino, B.; Eperon, G.E.; Snaith, H.J. Shunt-Blocking Layers for Semitransparent Perovskite Solar Cells. *Adv. Mater. Interfaces* **2016**, *3*, 1500837. [[CrossRef](#)]
37. Lee, K.-T.; Guo, L.J.; Park, H.J. Neutral- and Multi-Colored Semitransparent Perovskite Solar Cells. *Molecules* **2016**, *21*, 475. [[CrossRef](#)]
38. Chang, C.-Y.; Chang, Y.-C.; Huang, W.-K.; Lee, K.-T.; Cho, A.-C.; Hsu, C.-C. Enhanced Performance and Stability of Semitransparent Perovskite Solar Cells Using Solution-Processed Thiol-Functionalized Cationic Surfactant as Cathode Buffer Layer. *Chem. Mater.* **2015**, *27*, 7119–7127. [[CrossRef](#)]
39. Heo, J.H.; Jang, M.H.; Lee, M.H.; Han, H.J.; Kang, M.G.; Lee, M.L.; Im, S.H. Efficiency enhancement of semi-transparent sandwich type CH₃NH₃PbI₃ perovskite solar cells with island morphology perovskite film by introduction of polystyrene passivation layer. *J. Mater. Chem. A* **2016**, *4*, 16324–16329. [[CrossRef](#)]
40. Heo, J.H.; Han, H.J.; Lee, M.; Song, M.; Kim, D.H.; Im, S.H. Stable semi-transparent CH₃NH₃PbI₃ planar sandwich solar cells. *Energy Environ. Sci.* **2015**, *8*, 2922–2927. [[CrossRef](#)]
41. Eperon, G.E.; Burlakov, V.M.; Goriely, A.; Snaith, H.J. Neutral Color Semitransparent Microstructured Perovskite Solar Cells. *ACS Nano* **2014**, *8*, 591–598. [[CrossRef](#)]
42. Lynn, N.; Mohanty, L.; Wittkopf, S. Color rendering properties of semi-transparent thin-film PV modules. *Build. Environ.* **2012**, *54*, 148–158. [[CrossRef](#)]
43. Asahi, R.; Morikawa, T.; Irie, H.; Ohwaki, T. Nitrogen-Doped Titanium Dioxide as Visible-Light-Sensitive Photocatalyst: Designs, Developments, and Prospects. *Chem. Rev.* **2014**, *114*, 9824–9852. [[CrossRef](#)] [[PubMed](#)]
44. Zafar, M.; Yun, J.-Y.; Kim, D.-H. Performance of inverted organic photovoltaic cells with nitrogen doped TiO₂ films by atomic layer deposition. *Korean J. Chem. Eng.* **2018**, *35*, 567–573. [[CrossRef](#)]
45. Mahmood, K.; Sarwar, S.; Mehran, M.T. Current status of electron transport layers in perovskite solar cells: Materials and properties. *RSC Adv.* **2017**, *7*, 17044–17062. [[CrossRef](#)]
46. Kim, T.H.; Go, G.-M.; Cho, H.-B.; Song, Y.; Lee, C.-G.; Choa, Y.-H. A Novel Synthetic Method for N Doped TiO₂ Nanoparticles Through Plasma-Assisted Electrolysis and Photocatalytic Activity in the Visible Region. *Front. Chem.* **2018**, *6*, 458. [[CrossRef](#)]
47. Panepinto, A.; Dervaux, J.; Cormier, P.; Boujtita, M.; Odobel, F.; Snyders, R. Synthesis of p-type N-doped TiO₂ thin films by co-reactive magnetron sputtering. *Plasma Process. Polym.* **2020**, *17*, 1900203. [[CrossRef](#)]
48. Bag, A.; Radhakrishnan, R.; Nekovei, R.; Jeyakumar, R. Effect of absorber layer, hole transport layer thicknesses, and its doping density on the performance of perovskite solar cells by device simulation. *Sol. Energy* **2020**, *196*, 177–182. [[CrossRef](#)]
49. Yang, Q.; Yang, S.; Xi, T.; Li, H.; Yi, J.; Zhong, J. Gradient doping simulation of perovskite solar cells with CH₃NH₃Sn_{1-x}Pb_xI₃ as the absorber layer. *Curr. Appl. Phys.* **2022**, *44*, 55–62. [[CrossRef](#)]

50. Hussain, S.S.; Riaz, S.; Nowsherwan, G.A.; Jahangir, K.; Raza, A.; Iqbal, M.J.; Sadiq, I.; Naseem, S. Numerical Modeling and Optimization of Lead-Free Hybrid Double Perovskite Solar Cell by Using SCAPS-1D. *J. Renew. Energy* **2021**, *2021*, 6668687. [[CrossRef](#)]
51. Madan, J.; Singh, K.; Pandey, R. Comprehensive device simulation of 23.36% efficient two-terminal perovskite-PbS CQD tandem solar cell for low-cost applications. *Sci. Rep.* **2021**, *11*, 19829. [[CrossRef](#)]
52. Santos, I.M.D.L.; Cortina-Marrero, H.J.; Ruiz-Sánchez, M.; Hechavarría-Difur, L.; Sánchez-Rodríguez, F.; Courel, M.; Hu, H. Optimization of CH₃NH₃PbI₃ perovskite solar cells: A theoretical and experimental study. *Sol. Energy* **2020**, *199*, 198–205. [[CrossRef](#)]
53. Bhavsar, K.; Lapsiwala, P. Numerical simulation of perovskite solar cell with different material as electron transport layer using SCAPS-1D Software. *Semicond. Phys. Quantum Electron. Optoelectron.* **2021**, *24*, 341–347. [[CrossRef](#)]
54. Mamta; Maurya, K.; Singh, V. Sb₂Se₃ versus Sb₂S₃ solar cell: A numerical simulation. *Sol. Energy* **2021**, *228*, 540–549. [[CrossRef](#)]
55. Deepthi Jayan, K.; Sebastian, V.; Kurian, J. Simulation and optimization studies on CsPbI₃ based inorganic perovskite solar cells. *Sol. Energy* **2021**, *221*, 99–108. [[CrossRef](#)]
56. Raza, E.; Ahmad, Z.; Aziz, F.; Asif, M.; Ahmed, A.; Riaz, K.; Bhadra, J.; Al-Thani, N.J. Numerical simulation analysis towards the effect of charge transport layers electrical properties on cesium based ternary cation perovskite solar cells performance. *Sol. Energy* **2021**, *225*, 842–850. [[CrossRef](#)]
57. Lee, M.D.; Lee, G.J.; Nam, I.; Abbas, M.A.; Bang, J.H. Exploring the Effect of Cation Vacancies in TiO₂: Lithiation Behavior of n-Type and p-Type TiO₂. *ACS Appl. Mater. Interfaces* **2022**, *14*, 6560–6569. [[CrossRef](#)]
58. Vasu, K.; Sreedhara, M.B.; Ghatak, J.; Rao, C.N.R. Atomic Layer Deposition of p-Type Epitaxial Thin Films of Undoped and N-Doped Anatase TiO₂. *ACS Appl. Mater. Interfaces* **2016**, *8*, 7897–7901. [[CrossRef](#)]
59. Vasilopoulou, M.; Kelaidis, N.; Polydorou, E.; Soultati, A.; Davazoglou, D.; Argitis, P.; Papadimitropoulos, G.; Tsikritzis, D.; Kennou, S.; Auras, F.; et al. Hydrogen and nitrogen codoping of anatase TiO₂ for efficiency enhancement in organic solar cells. *Sci. Rep. Sci. Rep.* **2017**, *7*, 17839. [[CrossRef](#)]
60. Anitha, V.C.; Banerjee, A.N.; Joo, S.W. Recent developments in TiO₂ as n- and p-type transparent semiconductors: Synthesis, modification, properties, and energy-related applications. *J. Mater. Sci.* **2015**, *50*, 7495–7536. [[CrossRef](#)]
61. Mishra, A.; Bhatt, N.; Bajpai, A. Nanostructured superhydrophobic coatings for solar panel applications. In *Nanomaterials-Based Coatings*; Elsevier: Amsterdam, The Netherlands, 2019; pp. 397–424. [[CrossRef](#)]
62. Lakhdar, N.; Hima, A. Electron transport material effect on performance of perovskite solar cells based on CH₃NH₃GeI₃. *Opt. Mater.* **2020**, *99*, 109517. [[CrossRef](#)]
63. Jayan, K.D.; Sebastian, V. Comprehensive device modelling and performance analysis of MASnI₃ based perovskite solar cells with diverse ETM, HTM and back metal contacts. *Sol. Energy* **2021**, *217*, 40–48. [[CrossRef](#)]
64. Alipour, H.; Ghadimi, A. Optimization of lead-free perovskite solar cells in normal-structure with WO₃ and water-free PEDOT: PSS composite for hole transport layer by SCAPS-1D simulation. *Opt. Mater.* **2021**, *120*, 111432. [[CrossRef](#)]
65. Kumar, M.H.; Dharani, S.; Leong, W.L.; Boix, P.P.; Prabhakar, R.R.; Baikie, T.; Shi, C.; Ding, H.; Ramesh, R.; Asta, M.; et al. Lead-Free Halide Perovskite Solar Cells with High Photocurrents Realized Through Vacancy Modulation. *Adv. Mater.* **2014**, *26*, 7122–7127. [[CrossRef](#)]
66. Jeyakumar, R.; Bag, A. Methylammonium lead bromide based planar perovskite solar cells using various electron transport layers. *Sol. Energy* **2021**, *221*, 456–467. [[CrossRef](#)]
67. Singh, A.K.; Srivastava, S.; Mahapatra, A.; Baral, J.K.; Pradhan, B. Performance optimization of lead free-MASnI₃ based solar cell with 27% efficiency by numerical simulation. *Opt. Mater.* **2021**, *117*, 111193. [[CrossRef](#)]
68. Abdelaziz, S.; Zekry, A.; Shaker, A.; Abouelatta, M. Investigation of lead-free MASnI₃-MASnIBr₂ tandem solar cell: Numerical simulation. *Opt. Mater.* **2022**, *123*, 111893. [[CrossRef](#)]
69. Fatema, K.; Arefin, S. Enhancing the efficiency of Pb-based and Sn-based perovskite solar cell by applying different ETL and HTL using SCAPS-ID. *Opt. Mater.* **2022**, *125*, 112036. [[CrossRef](#)]
70. Karthick, S.; Bouclé, J.; Velumani, S. Effect of bismuth iodide (BiI₃) interfacial layer with different HTL's in FAPI based per-ovskite solar cell-SCAPS-1D study. *Sol. Energy* **2021**, *218*, 157–168. [[CrossRef](#)]
71. Lin, C.; Liu, G.; Xi, X.; Wang, L.; Wang, Q.; Sun, Q.; Li, M.; Zhu, B.; de Lara, D.P.; Zai, H. The Investigation of the Influence of a Cu₂O Buffer Layer on Hole Transport Layers in MAPbI₃-Based Perovskite Solar Cells. *Materials* **2022**, *15*, 8142. [[CrossRef](#)] [[PubMed](#)]

Disclaimer/Publisher's Note: The statements, opinions and data contained in all publications are solely those of the individual author(s) and contributor(s) and not of MDPI and/or the editor(s). MDPI and/or the editor(s) disclaim responsibility for any injury to people or property resulting from any ideas, methods, instructions or products referred to in the content.